Solubility of Amorphous Sodium Aluminosilicate and Zeolite A Crystals in Caustic and Nitrate/Nitrite-Rich Caustic Aluminate Liquors

Jonas Addai-Mensah,*,† Jun Li,† Scott Rosencrance,‡ and William Wilmarth‡

Ian Wark Research Institute, Australia Research Council Special Research Centre, University of South Australia, Mawson Lakes, Adelaide 5095, Australia, and Westinghouse Savannah River Company, Aiken, South Carolina

The solubility of amorphous sodium aluminosilicate solid and zeolite A crystals in sodium hydroxide and nitrated/nitrited sodium aluminate solutions has been determined at temperatures of (303.15, 338.15, and 403.15) K and as a function of solution NaOH, $NaNO_3$, $NaNO_2$, and Al(III) concentrations. Similar solubilities were measured when equilibrium was approached from below (via dissolution in undersaturated liquor) and above (by precipitation from supersaturated liquors). The solubility (expressed in terms of SiO_2 and Al(III) concentrations) increased monotonically with increasing temperature, solution ionic strength, and hydroxide concentration for both amorphous and zeolite A phases. However, the solubility decreased with increasing solution Al(III), NO_3^-, and NO_2^- concentrations and was significantly higher for the amorphous than the zeolite phase at all temperatures and solution conditions.

Introduction

During high-level nuclear waste (HLNW) processing, waste liquor concentration enhancement is achieved by continuous evaporation at elevated temperatures (e.g., (303−413) K). Sodium aluminosilicate (NAS) species in the concentrated (e.g., (6−12) mol·dm^{-3}) liquor that typically contains sodium, hydroxide, nitrite, nitrate, silica, and aluminate ions and complexes may become supersaturated at some point during the evaporation process. The supersaturation, together with the intensity of heat being transferred, often leads to the precipitation of unwanted and tenacious NAS scale at the surfaces of the evaporator heating tube and walls. Various NAS polytypes (e.g., amorphous solid/gel, zeolite A, and sodalite) displaying different thermodynamic stabilities and solubilities may precipitate as foulants, depending upon the processing conditions (e.g., solution species composition and concentration, temperature, and time). If uncontrolled, fouling may proceed at such a dramatic rate that a significant reduction in the evaporator's heat-transfer efficiency and liquor throughput, warranting plant shutdown, may occur. Furthermore, NAS scale formation may also facilitate the incorporation of solution trace radionuclide species (e.g., uranium), posing a serious criticality concern and technological challenge.

The formation of NAS polytypes under heat-exchanger conditions follows Oswald's rule of stages.[1] Under favorable conditions (e.g., high supersaturation and low temperature <338 K), the first NAS phase to precipitate in HLNW evaporators is the least thermodynamically stable amorphous solid. The amorphous phase invariably transforms in succession to the more stable zeolite, sodalite, and cancrinite crystalline phases with time.[1−6,19] Although the Si−Al−O framework elements of crystalline zeolite A and its amorphous precursor phase may be similar stoichiometrically,[7] their solid-state tetrahedral AlO_4 and SiO_4 clusters are structurally different. Depending upon the solution composition and conditions, a variety of zeolitic compounds may be crystallized.[2,3,5,7−10,19] In the present work, the zeolite phase of interest is Linde type A ($Na_{12}(Al_{12}Si_{12}O_{48})\cdot 27H_2O$), which is cubic with space group *Fm*3*c*.[11]

In previous studies, the solubility of amorphous and zeolite A phases has been determined under various solution conditions, as recourse to the literature shows.[1,6,8,12−16,19,20] The studies that indicate that zeolite A exhibits a significantly lower solubility than its amorphous precursor were, however, performed over a narrow range of temperatures (e.g., (338−353 K) and solution composition and/or low caustic ionic strength (e.g., (0.2−3.0) mol·dm^{-3}). These conditions make the relevance or applicability of the extant data to HLNW liquor processing very limited. Furthermore, to date the trends discerned from some of the reported data with the respect to the influence of the primary variables such as temperature and solution composition are conflicting or remain contentious or require further investigation. For example, temperature has been reported to have no effect on the solubility of amorphous NAS[16] and zeolite A[15] phases. However, other studies[6,8,12,14] clearly revealed conflicting temperature-dependent solubility behavior. The solubility of zeolite A was shown to increase with increasing temperature,[6,8,12−14] whereas for the amorphous phase, an inverse temperature effect has been reported.[12] No comprehensive study of the solubility of amorphous and zeolite species in NO_2/NO_3-rich caustic aluminate solutions has as yet been reported. The solubility of the NAS scale product is crucial for an accurate definition of the concentration driving force that underpins the mechanisms and kinetics of the precipitation and particulate fouling during HLNW processing and is the focus of our current studies.

In the present work, the equilibrium solubility determinations of amorphous and zeolite A phases in synthetic caustic and nitrated/nitrited caustic aluminate solutions were carried out under conditions close to those of Savan-

* Corresponding author. E-mail: jonas.addai-mensah@unisa.edu.au.
† University of South Australia.
‡ Westinghouse Savannah River Company.

10.1021/je049889f CCC: $27.50
Published on Web 09/24/2004

Table 1. Experimental Conditions Used in the Synthesis of Sodium Aluminosilicate Seed Particles

material	amorphous	zeolite A
C(NaOH)/mol·dm^{-3}	4.0	4.0
C(SiO_2)($Na_2O{\cdot}SiO_2{\cdot}5H_2O$)/mol·dm^{-3}	0.35	0.10
C(Al(III))/mol·dm^{-3}	0.47($Al(NO_3)_3{\cdot}2H_2O$)	1.67(γ-$Al(OH)_3$)
additive/mol·dm^{-3}	1.0($NaNO_3$) + 1.0($NaNO_2$)	0.38(Na_2CO_3)
temperature, T/K	298.15	357.15
reaction time, t/h	0.17	2.50

nah River (Aiken, SC) HLNW processing. The studies were aimed specifically at investigating the two NAS solid phases' SiO_2 and Al(III) equilibrium solubility as a function of

(i) temperature in the range of (303−403) K and

(ii) solution species concentrations C(NaOH) = (3.0−8.0) mol·dm^{-3}, $C(NaNO_3)$ = (0.0−2.0) mol·dm^{-3}, $C(NaNO_2)$ = (0.0−2.0) mol·dm^{-3}, and C(Al(III)) = (0.0−0.45) mol·dm^{-3}.

Experimental Procedure

Solution and NAS Seed Preparation. Pure, synthetic, optically clear caustic and SiO_2 free/supersaturated, nitrated/nitrated caustic aluminate solutions were used in the present work. They were prepared from analytical reagent grade sodium hydroxide (99% pure, 1.0% $NaCO_3$, Merck, Australia), aluminum metal (99.9% pure, 0.01% Si, Merck, Australia), aluminum nitrate (98.0% $Al(NO_3)_3{\cdot}9H_2O$, Merck, Australia), sodium nitrate (99.0% pure, Merck, Australia), sodium nitrite (97.0% pure, Merck, Australia), sodium metasilicate-pentahydrate (99.8% $Na_2O{\cdot}SiO_2{\cdot}5H_2O$, Merck, Australia), and Milli-Q water (specific conductivity < 0.5 μS cm^{-1}, pH 5.6, and surface tension 72.8 mN m^{-1} at 20 °C). Both NAS seed phases were freshly precipitated from highly supersaturated solutions whose compositions, temperatures, and reaction times are described in Table 1. For zeolite A crystal synthesis, additional reagents {gibbsite crystals (Hydral, 99.4% γ-$Al(OH)_3$, Alcoa, Arkansas) and anhydrous sodium carbonate (99.0% pure, Merck, Australia)} were used.

To prepare a 1-dm^3 nitrated/nitrited sodium aluminate solution, a known mass of NaOH was dissolved in 0.25 dm^3 of Milli-Q water in a partially sealed, caustic-resistant polymethyl pentene (PMP) 1-dm^3 beaker. This was followed by the slow addition of a known mass of Al metal (previously washed with ethanol to remove any organic contamination) under agitation of 300 rpm to dissolve and form an optically clear sodium aluminate solution. The PMP vessel was sealed with a lid containing pinholes to allow the escape of H_2 gas formed in the Al dissolution process while preventing both pressure buildup and CO_2 influx as well as minimizing water vapor loss. Known masses of $NaNO_3$ and $NaNO_2$ crystals were then added to the sodium aluminate solution for complete dissolution. The resulting solution was then transferred to a volumetric flask and that was filled up to the mark with Milli-Q water. For a SiO_2-supersaturated sodium nitrate/nitrite aluminosilicate solution, a known mass of sodium metasilicate dissolved in 0.05 dm^3 of Milli-Q water was added to the sodium aluminate solution before filling the flask up to the mark with Milli-Q water. All of the solutions were twice filtered through a 0.20-μm caustic-resistant Teflon membrane and used immediately to avoid aging. During preparation, the solutions were allowed as little exposure to air as possible and stored in airtight, sealed PMP containers to avoid CO_2 uptake.

Because of the ephemeral nature of the two NAS solids associated with solution-mediated phase transformation upon in situ aging, seed syntheses were carried out with great circumspection. After 10 min of massive precipitation of the amorphous NAS from highly supersaturated liquor, the resulting suspension was centrifuged to recover the solid phase. The short precipitation time ensured that no detectable transformation to zeolite A occurred.[1,19] Upon removal of the supernatant, the amorphous solid residue was redispersed in Milli-Q water and centrifuged repeatedly until it was free from alkali (final supernatant pH < 7.5). For zeolite A seed preparation, the crystals formed after 2.5 h of precipitation were separated from the supernatant by similar centrifugation and washing procedures. The washed solids were dried at 298.15 K for 4 days by silica gel desiccation prior to characterization (e.g., XRD and particle sizing) and use.

Experimental Run and Analyses. An Orbital incubator mixer (model OM 11, Ratek Laboratory Equipment Company, Australia) fitted with well-sealed 100-cm^3 caustic-resistant polymethyl pentene (PMP) containers (40 mm diameter) and a temperature control system was used to determine the solubilities at (303.15 and 338.15) K. The agitation speed was kept constant at 300 rpm. Preheated solutions (0.05 dm^3 of caustic and SiO_2-free/rich, nitrated/nitrited sodium aluminate) were seeded at 120 g NAS dm^{-3} solution. To determine the solubility at 403.15 K, a 0.6-dm^3 316 stainless steel, high-pressure autoclave (4843, Parr Instrument Company) fitted with a 0.5-dm^3 Teflon liner was used. An automatic proportional-integral-derivative control system was used to control the heating rate, the agitation speed, and the temperature of the autoclave. Temperature regulation was achieved through an external heater and internal cooling system. A central four-blade, 45°-pitch, two-tier impeller provided constant agitation at 300 ± 2 rpm, which ensured complete particle suspension and homogeneity. Previous[1,19,20] and ongoing NAS solubility and crystallization studies performed under similar conditions comprising a seed charge of (60−120) g·dm^{-3}solution, close to equilibrium supersaturations and the agitation range of (400−700) rpm, show that the concomitant energy dissipation rate operative in the autoclave does not cause any gross breakage, noticeable attrition and, hence, surface strain that might significantly impact solubility. Several solubility data produced at 300 rpm with the Orbital incubator mixer (without an impeller) and stirred autoclave under solution conditions were found to be substantially the same. The autoclave was prepressurized with H_2O-saturated N_2 gas at 400 kPa.The preheated nitrated/nitrited sodium aluminate solutions (0.25 dm^3) were placed in the stirred vessel.

For measurements from "below" equilibrium, 0.10 dm^3 of a preheated seed suspension (42 g of seed) was added to give a final volume of 0.35 dm^3 with a seed charge of 120 g·dm^{-3}. With measurements from "above", 0.05 dm^3 of preheated sodium metasilicate solution and 0.05 dm^3 of preheated seed suspension (42 g of seed) were added to the liquor sequentially once it had reached the correct temperature. The addition of the sodium metasilicate solution and seed slurry was carried out via a vertical, 0.1-dm^3 high-pressure steel tube whose bottom end is attached to the autoclave via a one-way valve. Discharge of the tube contents into the autoclave was achieved by metering compressed H_2O-saturated N_2 gas at a pressure exceeding the internal pressure of the autoclave through the top end of the tube. As soon as the temperature reached 403.15 K (typically within 30 s), the experimental time was set to zero. A small quantity of water (<2.0 cm^3) was found on the outside of the cooled autoclave liner at the completion

Table 2. Summary of the Sodium Aluminosilicate Seed Characteristics Used in Solubility Determinations

terms/seed type	amorphous	zeolite
unit cell parameter a/Å		24.60 ± 0.03
BET surface area/$m^2 \cdot g^{-1}$	79.8 ± 1.9	9.2 ± 0.5
particle Sauter mean diameter $D_{32}/\mu m$	0.90	2.21

Table 3. SiO_2 and Al(III) Equilibrium Solubility of Amorphous and Zeolite A Measured at Different Temperatures[a]

phase	T/K	C(NaOH)/ mol·dm^{-3}	solubility/10^{-3} mol·dm^{-3} $C(SiO_2)$	C(Al(III))
amorphous	303.15	3.00	70.2 ± 2.4	79.1 ± 2.3
	338.15	3.00	88.1 ± 2.5	94.9 ± 3.2
	403.15	3.00	111.9 ± 3.3	113.2 ± 2.9
	303.15	6.00	101.3 ± 2.9	98.9 ± 3.1
	338.15	6.00	207.4 ± 3.9	206.1 ± 4.3
	403.15	6.00	293.4 ± 3.9	295.2 ± 4.4
zeolite	303.15	3.00	11.8 ± 0.6	14.1 ± 1.3
	338.15	3.00	19.9 ± 0.7	26.9 ± 1.2
	403.15	3.00	30.9 ± 1.1	34.2 ± 1.4
	303.15	6.00	31.4 ± 1.0	39.9 ± 2.0
	338.15	6.00	44.0 ± 2.8	51.6 ± 2.5
	403.15	6.00	67.8 ± 2.4	71.5 ± 3.1

[a] Initial solution = (3.0 and 6.0) mol·dm^{-3} NaOH.

of the experiment at 403.15 K. This volume of condensed water vapor, being part of the initial solution volume of 350.0 cm^3, contributed to ~1.1% error (95% confidence interval) and, as a result, was considered minor to the overall uncertainties in the determination of the solution concentration.

Slurry samples were periodically removed and analyzed throughout the experimental run for SiO_2 and Al(III) concentrations, solid content, and solid-phase crystallographic or structural characteristics. The latter ensured that no noticeable phase transformation of the original seed occurred when equilibrium solubility was reached. The solution SiO_2, Al(III), and Na concentrations were analyzed by inductively coupled plasma (ICP, Spectro Analytical Instruments, Spectro SIM-SEQ ICP-OES). The solution NO_3/NO_2 concentration was determined via nitrogen assay using standard digestion/oxidation followed by segmented flow injection analysis.[21] The pure error in SiO_2 and Al(III) analyses was determined experimentally to be <3% by multiple ICP analysis of both the same solution and multiple solutions prepared from the same replicate liquor sample. For each solution, six samples were taken for ICP analysis. All equilibrium solubility measurements were replicated at least three times and, in most cases, determined from both dissolution and precipitation experiments. The uncertainties in the measured values reported were calculated on the basis of a 95% confidence interval from pure errors.

NAS seed particle characterization, before and after an experimental run, was achieved by powder X-ray diffraction (XRD) (Philips PW1050 X-ray generator equipped with Sietronic data collection), specific surface area by N_2 BET (Brunauer, Emmett, and Teller (1938) (Coulter Omnisorp 100, Hialeah, FL), and particle sizing (Malvern Mastersizer, U.K.) analyses. XRD patterns were collected on powdered samples in $^{\theta}/_{2\theta}$ scanning mode using Cu Kα radiation (wavelength λ = 1.5418 Å). The scan speed was 1° per min between (10 and 70) 2θ°. The zeolite A crystal unit cell was estimated manually from the dominant diffraction peaks and then refined using the NBS crystal data evaluation program.[17] The d spacing or 2θ data was

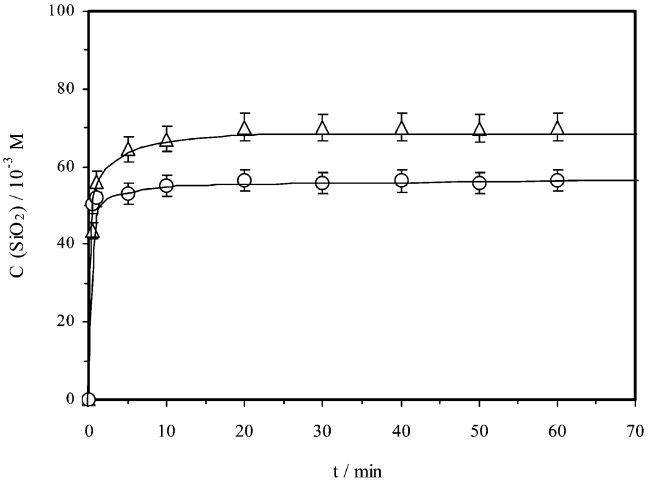

Figure 1. Variation of SiO_2 concentration with time during the dissolution of the amorphous in caustic (C(NaOH) = 3.0 mol·dm^{-3}) Δ and nitrited/nitrated caustic aluminate solutions (C(NaOH) = 8.0 mol·dm^{-3}, 2.0C($NaNO_3$) = C($NaNO_2$) = 2.0 mol·dm^{-3} and C(Al(III)) = 0.45 mol·dm^{-3})) ○ at 303.15 K.

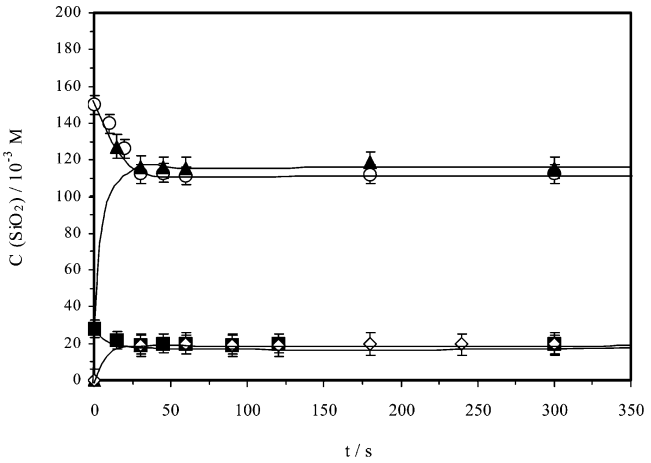

Figure 2. Solution SiO_2 concentration versus time during the NAS solubility determination by precipitation and dissolution at 338.15 K in solutions containing C(NaOH) = 4.0 mol·dm^{-3}, C($NaNO_2$) = 1.0 mol·dm^{-3}, C($NaNO_3$) = 1.0 mol·dm^{-3} and (a) C(Al(III)) = C(SiO_2) = 0.15 mol·dm^{-3} (○, amorphous precipitation) and C(Al(III)) = C(SiO_2) = 0.0 mol·dm^{-3} (▲, amorphous dissolution) and (b) C(Al(III)) = C(SiO_2) = 0.03 mol·dm^{-3}(■, zeolite A precipitation) and C(Al(III)) = C(SiO_2) = 0.0 mol·dm^{-3} (◇, zeolite A dissolution).

entered along with the estimated unit cell parameter. The unit cell parameter was adjusted by the program to give the lowest standard error. The amorphous product was shown to be completely X-ray indifferent. Scanning electron microscopy (Camscan CS44, Cambridge, U.K.) was used for imaging and energy dispersive spectroscopy (EDS) analysis of the seed particles. NAS particle sizing was carried out using a laser diffraction method (Malvern 2600C particle sizer, Malvern Instruments Ltd., Malvern, U.K.). The analysis was carried out in Milli-Q water with 5 min of sonication of the slurry in order to break up aggregates that resulted from drying. A summary of the seed particle information provided by the analyses is given in Table 2.

Results and Discussion

The solubility data obtained for amorphous and zeolite A is shown in Tables 3−5 and Figures 1−5. The results shown in Table 3 indicate typical solubility data obtained

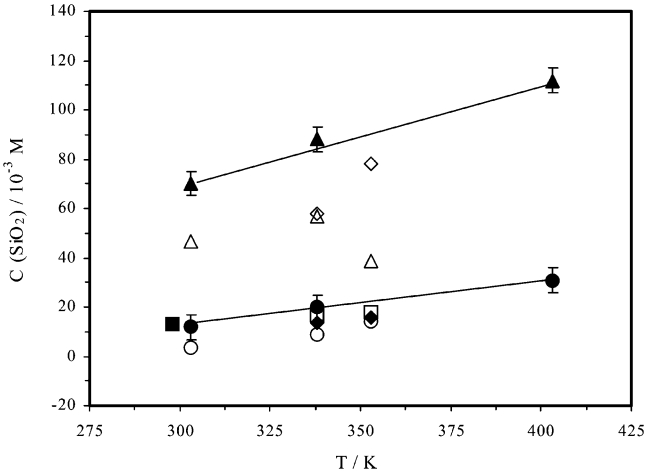

Figure 3. Equilibrium solubility of SiO_2 as a function of temperature for different NAS solid phases in solutions containing 3.0 mol·dm^{-3} NaOH (present work), 3.0 mol·dm^{-3} NaOH (Ejaz et al.[12]), 0.2 mol·dm^{-3} NaOH (Antonic et al.[8]), 5.0 mol·dm^{-3} solutions of NaCl + NaOH + $NaAlO_2$ (Pevzner et al.[16]), 2.0 mol·dm^{-3} NaOH (Cizmek et al.[15]), and 8.0 mol·dm^{-3} NaOH (Grujic et al.[6]). ▲, Amorphous (present work); △, amorphous (Ejaz et al.[12]); ◆, amorphous (Antonic et al.[8]); □, zeolite (Cizmek et al.[15]); ●, zeolite A (present work); ○, zeolite A (Ejaz et al.[12]); ■, amorphous (Pevzner et al.[16]), and △, zeolite A (Grujic et al.[6]).

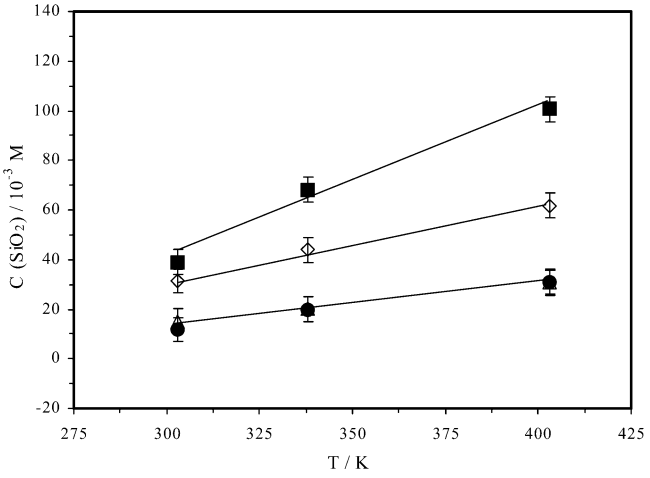

Figure 4. Variation of zeolite A crystals' equilibrium solubility of SiO_2 with temperature for different solutions: ●, C(NaOH) = 3.0 mol·dm^{-3}; ◇, C(NaOH) = 6.0 mol·dm^{-3}; △, C(NaOH) = 4.0 mol·dm^{-3}, $C(NaNO_3)$ = $C(NaNO_3)$ = 1.0 mol·dm^{-3}; and ■, C(NaOH) = 8.0 mol·dm^{-3} and $C(NaNO_3)$ = $C(NaNO_3)$ = 2.0 mol·dm^{-3}.

by approaching equilibrium from below via NAS seed dissolution in caustic solutions. Tables 4 and 5 also exhibit the results similarly obtained from caustic and nitrated/nitrited caustic solutions containing Al(III) in the range of (0−0.45) mol·dm^{-3}. Reported literature solubility data of relevance to the present work are also displayed in Figure 3 and Table 6 for comparison.

It is pertinent to note that with a high seed charge (120 g·dm^{-3} solution) strategy employed the equilibrium SiO_2 concentration was rapidly reached, typically within 2 h, as indicated by the plateau in Figures 1 and 2. Massive seeding at 360 g·dm^{-3} solution indicated the same equilibrium values seeding at 120 g·dm^{-3}. Therefore, this confirmed that the observed plateau SiO_2 concentration was indeed the equilibrium solubility. Approximately equal concentrations of SiO_2 and Al(III), indicative of acceptable congruency, were observed in initially Al(III)-free solutions

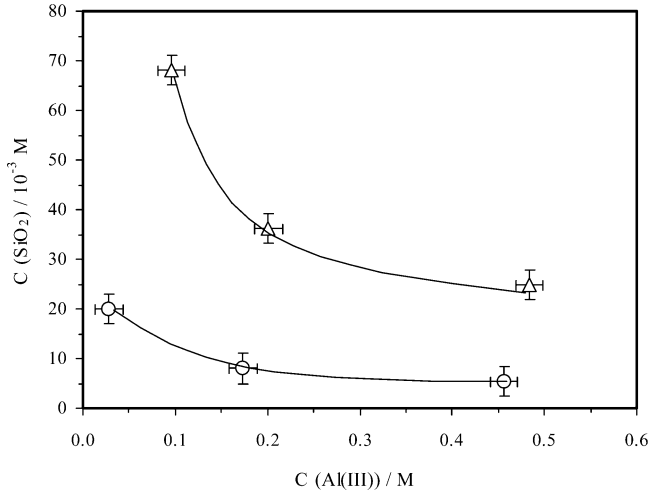

Figure 5. Zeolite A crystals' equilibrium solubility of SiO_2 as a function of Al(III) concentration at high and low solution ionic strength and 338 K: Δ, C(NaOH) = 8.0 mol·dm^{-3}, $C(NaNO_3)$ = $C(NaNO_3)$ = 2.0 mol·dm^{-3} and ○, C(NaOH) = 4.0 mol·dm^{-3}, $C(NaNO_3)$ = $C(NaNO_3)$ = 1.0 mol·dm^{-3}.

Table 4. SiO_2 and Al(III) Equilibrium Solubility of Amorphous and Zeolite A Measured at Different Temperatures[a]

phase	T/K	C(Al(III))/ mol·dm^{-3}	solubility/(10^{-3} mol·dm^{-3}) $C(SiO_2)$	C(Al(III))
amorphous	303.15	0.00	86.1 ± 3.0	79.1 ± 3.0
	338.15	0.00	116.3 ± 4.0	125.0 ± 4.0
	403.15	0.00	156.5 ± 4.3	158.9 ± 4.0
	303.15	0.15	55.8 ± 2.3	194.1 ± 4.2
	338.15	0.15	70.5 ± 3.0	205.2 ± 4.0
	403.15	0.15	89.2 ± 3.4	228.2 ± 4.5
	303.15	0.45	39.8 ± 1.7	470.3 ± 5.0
	338.15	0.45	45.4 ± 2.1	502.3 ± 6.3
	403.15	0.45	57.6 ± 2.1	510.8 ± 6.4
zeolite	303.15	0.00	15.1 ± 0.5	20.4 ± 1.3
	338.15	0.00	20.1 ± 1.1	26.3 ± 1.4
	403.15	0.00	30.6 ± 1.3	35.1 ± 2.0
	303.15	0.15	5.9 ± 0.3	148.5 ± 3.0
	338.15	0.15	9.2 ± 0.4	172.6 ± 4.2
	403.15	0.15	10.5 ± 0.4	164.8 ± 3.0
	303.15	0.45	4.2 ± 0.2	440.0 ± 5.3
	338.15	0.45	5.3 ± 0.2	456.1 ± 5.7
	403.15	0.45	7.4 ± 0.4	464.4 ± 5.8

[a] Initial solution composition C(NaOH) = 4.0 mol·dm^{-3}, $C(NaNO_3)$ = 1.0 mol·dm^{-3}, $C(NaNO_2)$ = 1.0 mol·dm^{-3}, C(Al(III)) = (0.0 0.15 and 0.45) mol·dm^{-3}.

at equilibrium. XRD analysis of the product particles showed that no detectable phase transformation occurred when equilibrium solubility was reached. XRD, EDS, and wet chemical analyses of the amorphous NAS and Linde type A zeolite products indicated a similar stoichiometric formula of $Na_{12}(Al_{12}Si_{12}O_{48})\cdot 27H_2O$, reconfirming the crystallographic characteristics of the seeds.

The solute species concentration (C) and mass balance analyses of the final solutions indicated that concentrations of NO_3^-, NO_2^-, and OH^- remained substantially unchanged whereas that of Na^+ slightly increased or decreased by an amount equivalent to the observed SiO_2 (the limiting reactant) solubility upon approach to equilibrium via dissolution and precipitation, respectively. Furthermore, good agreement was observed when the solubility data from both dissolution and precipitation were compared, although small but noticeable differences due to slightly higher values resulting from the dissolution method were observed (Figure 2). The difference in these values,

Table 5. SiO_2 and Al(III) Equilibrium Solubility of Amorphous and Zeolite A Measured at Different Temperatures[a]

phase	T/K	C(Al(III))/ mol·dm^{-3}	solubility/10^{-3} mol·dm^{-3} C(SiO_2)	C(Al(III))
amorphous	303.15	0.00	108.8 ± 3.5	109.1 ± 3.2
	338.15	0.00	257.8 ± 5.5	264.2 ± 6.0
	403.15	0.00		
	303.15	0.15	85.2 ± 3.5	220.1 ± 5.5
	338.15	0.15	193.7 ± 4.3	350.8 ± 5.5
	403.15	0.15		
	303.15	0.45	56.4 ± 2.7	510.6 ± 8.1
	338.15	0.45	144.7 ± 4.5	579.6 ± 7.6
	403.15	0.45		
zeolite	303.15	0.00	39.0 ± 2.0	45.8 ± 2.6
	338.15	0.00	68.1 ± 2.4	73.1 ± 2.9
	403.15	0.00	100.7 ± 3.6	100.2 ± 3.8
	303.15	0.15	22.1 ± 1.5	165.7 ± 4.5
	338.15	0.15	36.3 ± 1.9	280.9 ± 4.8
	403.15	0.15	54.0 ± 3.0	205.4 ± 4.5
	303.15	0.45	17.2 ± 1.0	460.3 ± 7.5
	338.15	0.45	24.9 ± 2.0	483.7 ± 6.5
	403.15	0.45	35.4 ± 2.2	488.0 ± 7.4

[a] Initial solution composition C(NaOH) = 8.0 mol·dm^{-3}, C($NaNO_3$) = 2.0 mol·dm^{-3}, C($NaNO_2$) = 2.0 mol·dm^{-3}, C(Al(III)) = (0.0, 0.15, and 0.45) mol·dm^{-3}.

which were found to be within 5% of each other, may be rationalized in terms of the variation in ionic strength of the liquors at equilibrium. As stated above, the ionic strength due to dissolution was slightly (2−4%) higher. Further analysis of the data shown below indicated that a marked ionic strength effect exists, with solubility increasing with increasing ionic strength, consistent with the observed difference between the data from dissolution and precipitation approaches. In general, the data depict several clearly defined trends reflecting solution composition, temperature, NAS seed structure type, and ionic strength influences, as enunciated below. In Figure 2, the first C(SiO_2) data point due to the dissolution of the amorphous phase measured within 15 s is notably higher than the others that follow. This may be ascribed to a particle size effect. As shown in Table 2, the amorphous seed particles, in contrast to the zeolite A seeds, were highly colloidal in size (D_{32} = 0.9 μm). Size analysis indicated that approximately 40 wt % of the particles were found to be <100 nm in size. Such highly colloidal particles were found to display not only to faster dissolution kinetics but also markedly higher solubility than coarser particles under similar caustic solution conditions. Thus, at the beginning, rapid dissolution dictated by the finer particles initially led to an instantaneous concentration higher than the solubility of the predominant coarser particles

NAS solubility is shown to be strongly dimorphic phase type dependent, with the amorphous exhibiting significantly higher solubility than zeolite A under similar solution conditions. Temperature had a profound effect on the solubility of both NAS phases, contrary to the findings of some reported studies.[15,16] A monotonic increase in solubility with increasing temperature was clearly observed under all solution conditions investigated (Figures 3 and 4). This observation is in good agreement with reported solubility studies of amorphous particles[8] and zeolite A.[6,12,14] A comparison between the present and reported data shown in Figure 3 indicates that whereas the agreement observed was good in some cases it was poor in others. The exact cause of the marked differences is as yet unknown.

The effect of Al(III) concentration on the solubility is indicated in Figures 5. In the C(Al(III)) range of (0.0−0.5) mol·dm^{-3}, SiO_2 solubility decreased in a distinctly nonlinear manner with increasing solution Al(III) concentration, in good agreement with the findings by Pevzner et al. (1974).[16] The decrease in solubility with increasing Al(III) concentration was greater at high than at low caustic and nitrate/nitrite concentration (Figure 5) and more pronounced for the amorphous than for the zeolite A phase (Tables 4 and 5). Increasing solution NaOH concentration from (3.0 to 6.0) mol·dm^{-3} resulted in the doubling of equilibrium SiO_2 and Al(III) solubility. However, the effect of NaOH on the solubility of the amorphous phase was less dramatic at 303.15 K. When the data obtained from types of solutions at similar ionic strengths (6.0 mol·dm^{-3} NaOH versus 4.0 mol·dm^{-3} NaOH, 1.0 mol·dm^{-3} $NaNO_3$ and 1.0 mol·dm^{-3} $NaNO_2$) are compared (Tables 4 and 5), it is clearly evident that the involvement of nitrate and nitrite ions, in lieu of hydroxide species, resulted in a substantial

Table 6. Reported Amorphous Sodium Aluminosilicate and Zeolite A Solubility Data

authors	experimental conditions C(NaOH)/mol·dm^{-3}	T/K	phase	solubility/10^{-3} mol·dm^{-3} C(SiO_2)	C(Al(III))
Ejaz et al., 1999	3.0	303.15	amorphous	46.53	34.50
	3.0	338.15	amorphous	56.67	41.43
	3.0	353.15	amorphous	38.60	28.95
Antonic et al., 1994	0.2	338.15	amorphous	13.6	11.6
	0.2	353.15	amorphous	15.5	13.0
Pevzner et al., 1974	5.0 + NaCl		amorphous	31.6	31.0
	+ $NaAlO_2$	298−338.15	amorphous	13.0	120.0
			amorphous	8.8	240
			amorphous	10.5	360
			amorphous	9.6	480
Ejaz et al., 1999	3.0	303.15	zeolite	3.25	4.29
	3.0	338.15	zeolite	8.85	8.86
	3.0	353.15	zeolite	14.04	12.86
Cizmek et al., 1991	1.0	338.15	zeolite	11.50	11.04
	2.0	338.15	zeolite	16.60	16.73
	1.0	353.15	zeolite	11.38	10.82
	2.0	353.15	zeolite	17.79	17.74
Grujic et al., 1989	8.0	338.15	zeolite	58	78
	8.0	358.15	zeolite	78	86
Caullet et al., 1979	0.5	298.15	zeolite	5.18	5.25
	0.5	333.15	zeolite	6.32	6.87

(~30−50%) reduction of the SiO_2 and Al(III) equilibrium solubility of both NAS phases.

In the present work, solvated, ion-paired, and free Na^+, OH^-, NO_3^-, NO_2^-, and $Al(OH)_4^-$ and SiO_2-containing solute species and their anionic complexes exist in solution under equilibrium conditions. Seemingly, the replacement of the OH^- ion, which is a strong base, with NO_3^-, NO_2^-, and $Al(OH)_4^-$ species that act as weak bases and the higher ionic strength of the solute markedly influenced the solid phase, solvent (water)−solute, and solute−solute interactions and had an adverse impact upon equilibrium SiO_2 solubility. It appears that at equilibrium Bronsted acid−base type interactions of which the presence of a stronger base results in the greater solubilization of sodium aluminosilicate species in solution occur. Furthermore, increasing the ionic strength of the solution by increasing NaOH, $NaNO_3$, and $NaNO_2$ concentrations led to a marked increase in solubility.

Conclusions

The SiO_2 and Al(III) equilibrium solubilities of amorphous NAS and zeolite A crystals have been measured as a function of temperature and NaOH, Al(III), $NaNO_3$, and $NaNO_2$ concentration under industrially relevant conditions. A significant effect of temperature, NAS seed phase type, solution hydroxide, nitrate, nitrite, and Al(III) concentration, and ionic strength on solubility is shown. The results enable a reliable supersaturation to be defined for quantifying the mechanisms and kinetics of amorphous and zeolite precipitation and fouling behavior.

The solubility of both amorphous and zeolite A phases increased monotonically with increasing temperature, solution ionic strength, and hydroxide concentration but decreased with increasing solution Al(III), NO_3^-, and NO_2^- concentrations. Significantly higher solubilities were observed for the amorphous than the zeolite phase at all temperatures and solution conditions.

Acknowledgment

Useful discussions with Walter Tamosaitis are gratefully acknowledged.

Literature Cited

(1) Barnes, M. C.; Addai-Mensah, J.; Gerson, A. R. The Mechanism of the Sodalite to Cancrinite Phase Transformation in Synthetic Spent Bayer Liquor. *Microporous Mesoporous Mater.* **1999**, *31*, 287−302.
(2) Angell, C. L.; Flank, W. H. Mechanism of Zeolite A Synthesis. *Mol. Sieves − 2, Int. Conf. 4th* **1977**, 194−206.
(3) Barrer, R. M. *Hydrothermal Chemistry of Zeolites*; Academic Press: London, 1982.
(4) Walton, R. I.; Millange, F.; O'Hare, D. An in Situ Energy-Dispersive X-ray Diffraction Study of the Hydrothermal Crystallization of Zeolite A. 1. Influence of Reaction Conditions and Transformation into Sodalite. *J. Phys. Chem. B* **2001**, *105*, 83−90.
(5) Marui, Y.; Irie, R.; Takiyama, H.; Uchida, H.; Matsuoka, M. Analysis of Nucleation of Zeolite A from Clear Solutions. *J. Cryst. Growth* **2002**, *237−239*, 2148−2152.
(6) Grujic, E.; Subotic, B.; Despotovic, L. A. Transformation of Zeolite A into Hydroxysodalite. III. The Influence of Temperature on the Kinetics of Transformation. In *Zeolites: Facts, Figures, Future*, Proceedings of the 8th International Zeolite Conference, Amsterdam, The Netherlands, July 10−14, 1989; Jacobs, P. A., van Santen, R. A., Eds.; Elsevier, Amsterdam, 1989; pp 261−270.
(7) Zhdanov, S. P. In *Some Problems of Zeolite Crystallization, Molecular Sieve Zeolites I*; Gould, R. F., Ed.; Advances in Chemistry Series; American Chemical Society: Washington, DC, 1971; Vol. 10120-43.
(8) Antonic, T.; Cizmek, A.; Subotic, B. Dissolution of Amorphous Aluminosilicate Zeolite Precursors in Alkaline Solutions. *J. Chem. Soc., Faraday Trans.* **1994**, *90*, 3725−3728.
(9) Gasteiger, H. A.; Frederick, W. J.; Streisel, R. C. Solubility of Aluminosilicates in Alkaline Solutions and a Thermodynamic Equilibrium Model. *Ind. Eng. Chem. Res.* **1992**, *31*, 1183−1190.
(10) Subotic, B.; Graovac, A. Kinetic Analysis of Autocatalytic Nucleation during Crystallization of Zeolites. In *Zeolites: Synthesis, Structure, Technology, and Application*, Proceedings of an Internation Symposium, September 3−8, 1984; Drzaj, B., Hocevar, S., Pejovnik, S. Eds.; Elsevier: Amsterdam, 1985; pp 199−206.
(11) Meier, W. M.; Olson, D. H.; Baerlocher, C. *Zeolites* **1996**, 171.
(12) Ejaz, T and Jones, A. G. Solubility of Zeolite A and Its Amorphous Precursor under Synthesis Conditions. *J. Chem. Eng. Data* **1999**, *44*, 574−576.
(13) Sefcik, J.; McCormick, A. V. What Is the Solubility of Zeolite A? *Microporous Mater.* **1997**, *10*, 173−179.
(14) Caullet, P.; Guth, J. L.; Wey, R. Solubility of Zeolites 4A and 13X in the Aqueous Basic Solutions and Thermodynamics of Dissolution. *C. R. Seances Acad. Sci., Ser. D* **1979**, *288*, 1059−1062.
(15) Cizmek, A.; Komunjer, L.; Subotic, B. Kinetics of Zeolite Dissolution: Part 1. Dissolution of Zeolite A in Hot Sodium Hydroxide. *Zeolites* **1991**, *11*, 258−264.
(16) Pevzner, I. Z.; Eremin, N. I.; Rozen, Y. B.; Kolobov, N. P.; Mironov, V. E., State of Silicon in Aluminate Solutions. *Zh. Prikl. Khim.* **1974**, *12*, 2847−2849.
(17) Mighell, A. D.; Hubbard, C. R.; Stalick, J. K. Technical Note 1141; National Bureau of Standards, 1981.
(18) Brunauer, S.; Emmett, P. H.; Teller, E. Adsorption of Gases in Multimolecular Layers. *J. Am. Chem. Soc.* **1938**, *60*, 309−319.
(19) Barnes, M. C.; Addai-Mensah, J.; Gerson, A. R.; Smart, R. St. C. The Solubility of Sodalite and Cancrinite in Synthetic Spent Liquor and the Mechanism and Kinetics of the Sodalite to Cancrinite Phase Transformation. *Light Met.* **1999**, 131−140.
(20) Barnes, M. C.; Addai-Mensah, J.; Gerson, A. R. The Solubility of Sodalite and Cancrinite in Synthetic Spent Bayer Liquor. *Colloids Surf., A* **1999**, *157*, 101−116.
(21) *Standard Methods For the Examination of Water and Wastewater*, 20th ed.; Clesceri, L. S., Greenberg, A. E., Eaton, A. D., Eds.; American Public Health Association: Washington, DC, 1998; 4-100−4-128.

Received for review March 19, 2004. Accepted August 12, 2004. Financial support was provided by Westinghouse Savannah River Company (Aiken, SC).

JE049889F